An Exploratory Non-Destructive Provenance Analysis of Two Middle Archaic Greenstone Pendants from Little Salt…

Article *in* Geoarchaeology · March 2014

DOI: 10.1002/gea.21470

CITATIONS
5

READS
66

4 authors, including:

Robert H. Tykot
University of South Florida
241 PUBLICATIONS **2,158** CITATIONS

SEE PROFILE

Research Article

An Exploratory Non-Destructive Provenance Analysis of Two Middle Archaic Greenstone Pendants from Little Salt Spring, Florida, USA

Michael F. Bonomo,[1,*] Justin P. Lowry,[2] Robert H. Tykot,[3] and John A. Gifford[4]

[1]Department of Geological & Environmental Sciences, Stanford University, Stanford, California
[2]Department of Sociology & Anthropology, George Mason University, Fairfax, Virginia
[3]Department of Anthropology, University of South Florida, Tampa, Florida
[4]Department of Anthropology, University of Miami, Coral Gables, Florida

Correspondence
*Corresponding author;
E-mail: bonomo@stanford.edu

Received
11 March 2011
Revised
26 November 2013
Accepted
27 November 2013

Scientific editing by Drew Coleman

Published online in Wiley Online Library (wileyonlinelibrary.com).

doi 10.1002/gea.21470

Test excavations in 2005 and 2006 of the Little Salt Spring mortuary pond in Southwest Florida (USA) yielded two exotic stone pendants indirectly dated to the Middle Archaic (7000–5000 ^{14}C year B.P.). Hand-specimen petrographic observation, combined with non-destructive environmental scanning electron microscopy, X-ray fluorescence spectroscopy, and whole-rock X-ray diffraction, identified the pendants as (1) a mica-plagioclase-edenite amphibolite or schist and (2) an intermediate pyroxene- and/or amphibole-bearing granitoid. Provenance was broadly constrained to a number of potential sources in the southern Appalachian Piedmont of the United States (at a minimum distance of 650 km from the archaeological findspot) utilizing the United States Geological Survey's National Geologic Map Database lithologic search tool (GEOLEX) and Mineral Resources On-Line Spatial Data GIS database. Due to the absence of lithologic matches within the state of Florida, we propose that the two artifacts most likely arrived at Little Salt Spring through down-the-line exchange of materials of prestige value with geologic origins in the southern Appalachian Piedmont, arguing for the existence of small-scale long-distance lithic exchange networks reaching into Archaic Florida. From a methodological standpoint, this study illustrates the potential utility of data collected under nonideal, non-destructive analytical conditions for deriving meaningful archaeological interpretations. © 2014 Wiley Periodicals, Inc.

INTRODUCTION

The ability to identify the raw material sources of cultural heritage materials has developed into an important tool of archaeological inquiry. In addition to direct implications regarding resource procurement strategies (Parish, Swihart, & Li, 2013), provenance determinations often serve as proxies for a variety of human behaviors, interactions, and beliefs, including mobility and territoriality (Burke, 2006), directionality and volume of exchange networks (Stoltman et al., 2005), and landscape perceptions (Vicens et al., 2010; Michelaki, Hancock, & Braun, 2012). The employment of non- or minimally-destructive technologies for archaeological analysis has flourished in the recent literature in response to technological advancements and novel adaptations of existing methods (e.g., Nevin, Spoto, & Anglos, 2012; Parish, Swihart, & Li, 2013), and such techniques are preferred, if not required, in instances where traditional destructive sample preparation is impermissible or where such preparation and analysis is time- or cost-prohibitive given a desired sampling volume or strategy (Lundblad, Mills, & Hon, 2008; Potts, 2008; Artioli & Angelini, 2011).

Combined approaches to archaeological sourcing are commonly espoused, as the synthesis of multiple classes of data carries a greater potential for making more secure source assignments (Neff, 2012; Nazaroff, Baysal, & Çiftçi, 2013). With respect to lithic sourcing, a combined approach will generally incorporate both geochemical and petrographic data. However, the non-destructive potential of certain instrumental techniques for providing

reliable and interpretable geochemical or petrographic information may not always be apparent due to a lack of representation in the archaeological literature. In particular, while scanning electron microscopy (SEM) and X-ray diffraction (XRD) are typically applied to archaeological samples that have undergone destructive preparation involving the powdering, thin sectioning, or sputter coating of samples (e.g., Šegvić et al., 2012), these two basic techniques are also capable of being applied non-destructively in the analysis of cultural heritage materials.

Here we present the results of a combined non-destructive geochemical and mineralogical study aimed at determining the provenance of two archaeological greenstone pendants from the Paleoindian- to Archaic-period Little Salt Spring site in Florida, USA. Our use of the term "greenstone" herein corresponds to a loose archaeological definition rather than a strict geological definition carrying mineralogical or petrogenetic significance. The pendants reported here represent two of only three archaeological greenstones discovered among Florida's Archaic sites to date, and are among Florida's oldest ceremonial artifacts to be analyzed for provenance (the third pendant, from the Republic Groves site in Hardee County, Florida [8HR4], is, at the time of writing, on display in an exhibit at the University of Florida's Museum of Natural History in Gainesville). This case study serves not only as an interpretation of early practices of exotic stone resource acquisition among Florida's Archaic peoples, but on a broader scale as a demonstration of the potential utility of non-destructive SEM and XRD methodologies in the field of archaeology.

ARCHAEOLOGICAL CONTEXT

Little Salt Spring (8SO18) in southern Sarasota County, Florida, USA (Figure 1), is a flooded spring-fed sinkhole once used as a mortuary pond by Archaic-period groups (Clausen et al., 1979; Wentz & Gifford, 2007); additionally, it may have functioned as a freshwater oasis and natural animal trap during the Paleoindian and early Archaic periods (Gifford, 1993). Well-preserved organic artifacts made of animal bone and antler, as well as ecofacts (wood, charcoal, and peat) have yielded ^{14}C ages for the occupations at Little Salt Spring ranging from 12,000–9000 ^{14}C year B.P. for Paleoindian cultural remains and 6800–5200 ^{14}C year B.P. for Archaic artifacts (Clausen et al., 1979). Approximately 100 more radiocarbon determinations since 1992 indicate a roughly similar range of radiocarbon dates from 12,500–6000 ^{14}C year B.P.

During underwater test excavations on the east slope of the upper basin of Little Salt Spring in 2005, University of Miami research divers and volunteer divers from the Florida Aquarium recovered a stone pendant (designated W24S04A04) from a 4 × 4 m survey square in 7.6 m of water. A second, smaller stone pendant (W24N04WA03) was recovered in June of 2006 on the east basin slope approximately 10 m north of the findspot of the first pendant in survey square W24N04W. Artifacts recovered from this portion of the upper basin, as well as some disarticulated and commingled human skeletal remains, are believed to represent Middle Archaic burials that have naturally eroded from the shallow uppermost slope of the basin and, over the millennia, migrated downslope and over the drop-off under the influence of gravity. The two pendants are indirectly dated to the Middle Archaic period by means of ^{14}C dating of other artifacts from the same survey square in which the smaller pendant was found.

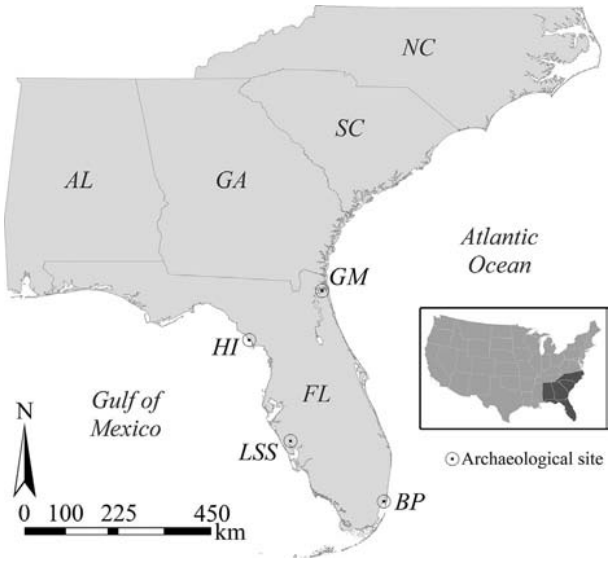

Figure 1 Study area in the southeastern United States, showing Florida archaeological sites mentioned in the text. *LSS* = Little Salt Spring (8SO18); *BP* = Brickell Point (8DA12); *HI* = Hog Island/Grave Yard Island (8CI220); *GM* = Goodman Mound.*FL* = Florida; *AL* = Alabama; *GA* = Georgia; *SC* = South Carolina; *NC* = North Carolina.

MATERIALS

W24S04A04

The first of the pendants, W24S04A04 (subsequently referred to as A04; Figure 2A) is likely an altered amphibolite or amphibole schist. The mass of A04 was measured at 12.0 g with an average specific gravity of $G = 2.84$ over eight replicate measurements. It is polished, biconically drilled, and carved into a parabolic curve extending distally from the drilled end. Its maximum length is 49 mm and 28 mm in width across its proximal (drilled) end.

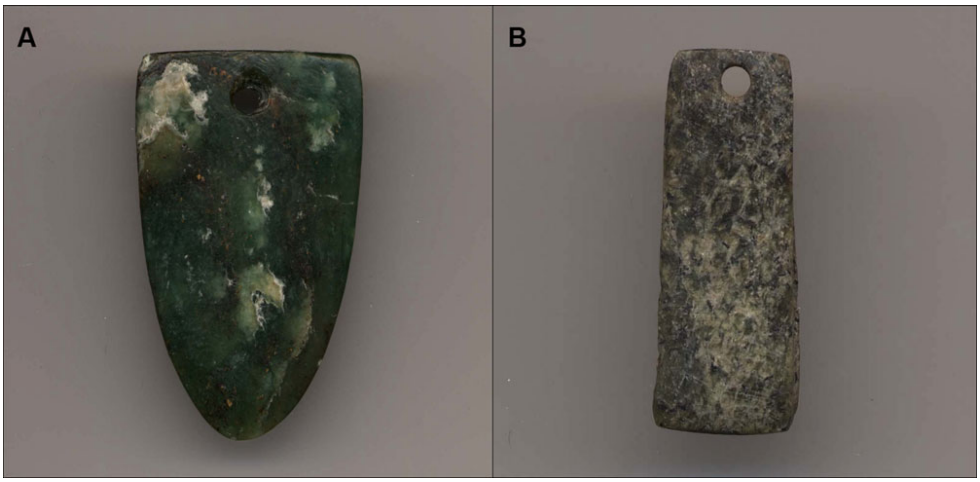

Figure 2 (A) Pendant W24S04A04 (vertical axis approximately 49.0 mm in length). (B) Pendant W24N04WA03 (vertical axis approximately 26.5–27.0 mm in length).

W24N04WA03

The second pendant, tagged as W24N04WA03 and subsequently referred to as A03 (Figure 2B), was identified as a coarse-grained pyroxene- and/or amphibole-bearing granitoid. It is roughly rectangular in shape, with a length ranging from 26.5 to 27 mm. The mass of A03 was measured at 1.8 g with an average specific gravity of $G = 2.57$ over five replicate measurements. The pendant is also polished and biconically drilled at one end. Both thickness and width of the stone increase in the direction distal to the drill hole, with a width of 8.5 mm and thickness of 2 mm near the drill hole and a width of 10 mm and thickness of 3 mm at the distal end.

METHODOLOGY

General Methods

Due to the rarity and value of these artifacts, only non-destructive analytical techniques were employed. Pendants A03 and A04 were analyzed using a combination of environmental SEM coupled with energy-dispersive X-ray fluorescence spectroscopy (ESEM-EDS), laboratory-based and portable XRF (XRF and pXRF), whole-rock XRD, macroscopic petrographic observation, and whole-rock specific gravity analysis.

Environmental Scanning Electron Microscopy

The application of SEM to the sourcing of geological raw materials has long been realized (e.g., Freestone & Middleton, 1987). However, with respect to lithics, the majority of SEM methodologies detailed in the archaeological literature involve destructive sampling of the materials under study (either fragmentation or thin sectioning) necessitated by small sample chamber dimensions relative to a larger sample (Janssens et al., 2000; Mantler & Schreiner, 2000). The non-destructive capabilities of SEM instruments are therefore dependent on instrument-specific sample chamber size limitations, and also on the availability of a detector capable of operating in a gaseous atmosphere as opposed to a vacuum. Such variants of the SEM are termed ESEMs, and unlike traditional SEM instruments, are capable of analyzing materials without the need for contaminative sputter coating or other forms of insulation or pretreatment (Danilatos, 1991). ESEM-EDS analyses were performed on both archaeological pendants at the University of Miami's Center for Advanced Microscopy (UMCAM) on the Coral Gables, Florida, campus on an FEI XL-30 field emission environmental scanning electron microscope. ESEM operation was conducted in an atmosphere at 1.4 Torr, and *in situ* qualitative chemical analyses were obtained via EDS operating with an accelerating voltage of 20.0 kV and a beam diameter of 3 μm.

X-ray Fluorescence and Portable XRF

XRF has been widely utilized in the archaeological field to provide both qualitative and quantitative measures of the elemental compositions of materials and potential sources (Shotton & Hendry, 1979; for a recent example, see Nazaroff, Baysal, & Çiftçi, 2013). XRF theory is well-established in the literature, and readers are referred to the descriptions of the theory and principles of XRF presented by Bertin (1970) and Potts (1987).

Multiple independent qualitative XRF analyses were performed on A04: one at the State University of New York at Albany's (SUNY—Albany) Ion Beam Laboratory and a second at the University of South Florida's (USF) Laboratory for Archaeological Sciences. Analyses of both artifacts were undertaken with no destructive sample preparation. The XRF instrument at SUNY—Albany's Ion Beam Laboratory has an estimated resolution of 165 eV for Fe at 6.40 kV. The sample chamber was not evacuated. Characteristic X-rays from the sample were detected by a Si(Li) detector, counted, and sorted by a multichannel analyzer. The analytical procedure was based on previous experimental XRF work (Kuhn & Lanford, 1987; Stevenson, Klimkiewicz, & Scheetz, 1990; Hermes & Ritchie, 1997; Williams-Thorpe, Potts, & Webb, 1999). Two XRF analyses were performed on A04 at the Ion Beam Laboratory with a scan time of 240 minutes each, one with a Sn target and the other with a Ta target. The Sn target yielded better results, as several of the trace elements identified in the scan would have been indistinguishable if analyzed with the Ta target alone. Elemental peaks were identified with the computer programs Analysis and AXIL. XRF analysis of A03 was not conducted at SUNY—Albany.

The analysis of both A04 and A03 at the Laboratory for Archaeological Sciences at USF utilized a Bruker Tracer III series handheld XRF (pXRF) analyzer with settings (40.00 kV accelerating voltage, 10.00 μA current, no vacuum) and filters aimed at quantitatively measuring the presence of Fe and trace elements Rb, Sr, Y, Zr, and Nb. Spectra were collected for 300 seconds each and raw photon counts were converted to part-per-million concentrations utilizing the five UMC calibration program developed at the University of Missouri—Columbia and distributed by Bruker Corporation. The relative proportions of elements such as K, Ca, and Ti were also recorded, though calibrations were not available for these elements on this instrument using this particular configuration. For general considerations relating to the applications (and limitations) of pXRF, readers are referred to Potts and West (2008), and Shugar and Mass (2012).

X-ray Diffraction

XRD is a spectroscopic technique that measures the distance, d, between lattice planes in a crystalline sample by relating this spacing between planes to the wavelength (λ) and angle (θ) of the incident X-rays according to the Bragg equation

$$n\lambda = 2d\sin\theta \quad (1)$$

where n is an integer representing the number of wavelengths. Different minerals have characteristically different d spacings between particular crystallographic planes, allowing minerals to be identified from a diffractogram (Moore & Reynolds, 1997). Mineralogical identification via XRD is often viewed as "unreliable" for objects with curved, complex, or otherwise nonflat surfaces (Zhigachev, 2013), usually necessitating the destructive preparation of pressed powders, pellets, or slides (readers are referred to Moore & Reynolds, 1997, for more detailed information on the general theory of XRD and common sample preparation techniques). As the accuracy of the observed d spacing is highly dependent on maintaining a precise geometric orientation between the incident source X-rays, the sample plane, and the detector, it is inevitable that peaks produced in any nondestructive whole-rock scans of curved surfaces will not be perfect matches with published powder diffraction data, even with the application of correction procedures. However, while uncommon, precedent does exist for the careful archaeological interpretation of non-destructive whole-rock XRD diffractograms, with Steponaitis et al. (2011: 86) asserting that any "interpretive difficulties . . . [are] easily mitigated with a detailed visual examination of the diffraction patterns, coupled with the information gained from the hand-sample petrology."

Non-destructive XRD analysis was performed on pendant A04 only at the University of Georgia's Department of Geology on a Bruker D8-Advance diffractometer, with the results processed using DIFFRAC.SUITE TOPAS software; the small size of A03 relative to the XRD sample holder did not allow the artifact to be adequately oriented for analysis. For the XRD analysis of A04, no sample preparation was undertaken other than the surficial application of a powdered ZnO analytical standard (National Institute of Standards and Technology Standard Reference Material 674a). The standard was smoothed onto a portion of the surface of the artifact in an attempt to correct for sample displacement caused by the curved surface of the artifact extending inside the diffractometer's focusing circle and was removed by rinsing in water following the analysis. The use of internal standards, where the standard is mixed with the powdered sample, is a common analytical technique in XRD (e.g., Hurst, Schroeder, & Styron, 1997; Środoń et al., 2001). The powdering of A04, however, was not an option; hence, the standard was applied externally and smoothed onto the surface of the artifact as best as possible. Similar methods are presented in Steponaitis et al. (2011). Application of the standard for XRD was conducted only *after* the ESEM-EDS and XRF chemical analyses were performed in order to avoid spectral artifacts resulting from any potential surficial contamination by Zn.

Two XRD analyses were performed on A04 using Co$K_{\alpha 1}$ radiation with a wavelength of 1.79 Å, an

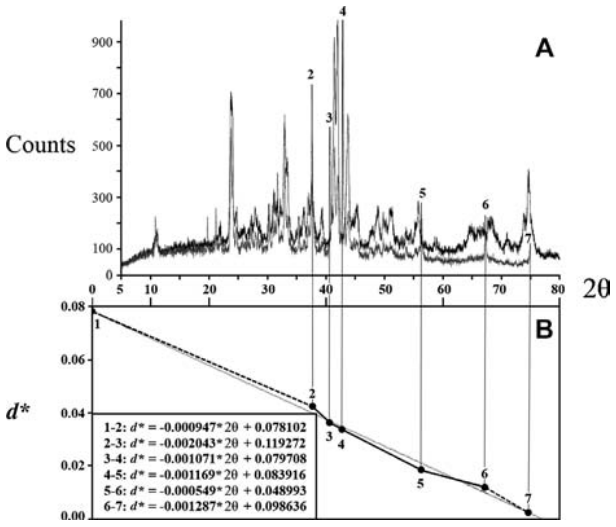

Figure 3 (A) XRD diffractogram of A04. Axes are in units of 2θ angle (in degrees, *x*-axis) and counts (*y*-axis). The darker, higher intensity pattern was produced prior to the application of the NIST SRM 674a ZnO standard. The lighter, lower intensity pattern was produced after surficial application of the standard. (B) *d* Spacing corrections applied to peaks produced in the XRD diffractogram of A04. Axes are in units of 2θ angle (in degrees, *x*-axis, aligned with the *x*-axis in Figure 3A) and correction, *d**. Numbered data points correspond to NIST SRM 674a ZnO standard peaks identified in the diffractogram: 2—(1 0 0) plane; 3—(0 0 2); 4—(1 0 1); 5—(1 0 2); 6—(1 1 0). Points 1 and 7 correspond to the beginning and end of the scan, and are not ZnO peaks. Linear equations of the form $d^* = mx\,2\theta + b$ represent the correction equations applied to peaks identified along each segment of the scan (i.e., between ZnO peaks), and were used to obtain the *d* spacings given in Table II. Vertical tie lines connecting points 2–6 in Figure 3B to peaks in the diffractogram in Figure 3A identify the ZnO peaks in the scan; the tie line at point 7 indicates the end of the scan.

accelerating voltage of 40 kV and a current of 35 mA, at a scan speed of 1° 2θ per minute with a step increment of 0.02° from 5.00° to 75.00° 2θ. Results obtained on the instrument are precise to at least four decimal places. One scan was run prior to the application of the ZnO standard and the other after the standard was applied (Figure 3A). In this manner, the ZnO peaks were easily identified in the scan and the appropriate corrections were applied to the peak *d* spacings from the artifact to correct for sample displacement created by the irregular shape of the pendant relative to the sample holder (Table I). Separate corrections were calculated for each segment of the scan, that is, between each set of adjacent data points for the ZnO standard by means of a linear regression (Figure 3B). It should be noted that peaks for the ZnO standard covered only the range of *d* from approximately 1.62–2.61 Å, and that 25 peaks were identified within the range $\sim 14 > d > 2.61$ Å (though only four peaks were detected at $d > 5$ Å), while two peaks were identified at $d <$ 1.62 Å. To obtain corrections outside of the range covered by the standards, a linear regression was performed using all data points from the standard (the solid gray line in Figure 3B), and a segment was formed between (1) the calculated correction at $2\theta = 0°$ (at a *d* correction of approximately 0.0781 Å, as calculated from the regression; the point labeled "1" in Figure 3B) and the first ZnO peak in the scan (at 37.57° and 0.0425 Å, point "2"), and (2) between the last ZnO peak in the scan (at 67.27° and 0.0121 Å, point "6") and the regression-calculated *d* correction at the end of the scan (75.00° and 0.0021 Å, point "7"). As such, more confidence can be placed in the accuracy of the corrections applied within the range covered by the ZnO standard; the least confidence is placed on those values approaching $d = 14$ Å.

Forty minerals with known green color variants (e.g., several pyroxene, amphibole, serpentine, and chlorite-group minerals), or otherwise common rock-forming minerals (e.g., quartz, feldspars, and micas), were selected from the Mineralogical Society of America's (MSA) Crystal Structure Database (http://www.minsocam.org/MSA/crystal_database.html; Downs & Hall-Wallace, 2003) for comparison with the corrected peak *d* spacings obtained from the diffractogram of pendant A04 (see Table III for the complete list of minerals). Automated search-match algorithms were not utilized as such algorithms rely on peak intensity, which was considered unreliable in the artifact scan, in addition to *d* spacings. Mineral phases were assigned to peaks on the arbitrary basis of a "good" match constituting a corrected *d* spacing occurring within 0.0009 Å of a published *d* spacing for that mineral, with the potential for multiple phases to be preliminarily assigned to a single peak. In addition, the "best" match or matches were defined as the phases with the closest published *d* spacing relative to a given corrected *d* spacing from the diffractogram. The 40 individual mineral phases were then grouped into general mineral groups (e.g., micas, pyroxenes, amphiboles, etc.) for subsequent determination of which mineral groups could best account for the remaining non-ZnO peaks in the diffractogram.

Specific Gravity

Specific gravity (*G*) is a unitless ratio of a material's mass to that of an equal volume of water (Klein, 2002: 33). Specific gravity measurements of A03 and A04 were conducted at the University of Georgia through the hydrostatic weighing method with a digital apparatus (see Rapp, 2009: 26). Values were calculated by measuring each artifact's mass in air (m_a) followed by measuring its mass as suspended in water (m_w) at room temperature

Table I Certified, observed, and corrected XRD *d* spacings for NIST SRM 674a standard applied to artifact A04.

NIST SRM 674a (plane)	$2\theta_{CuK\alpha}(^{o})_{cert}$[a] $\lambda = 1.54$ Å	$2\theta_{CoK\alpha}(^{o})_{cert}$[b] $\lambda = 1.79$ Å	$2\theta_{CoK\alpha}(^{o})_{obs}$[c] $\lambda = 1.79$ Å	d_{obs} (Å)[d]	$d_{corrected}$ (Å)[e]
1 0 0	31.70	37.02	37.57	2.7778	2.8204
0 0 2	34.36	40.16	40.71	2.5717	2.6079
1 0 1	36.18	42.32	42.88	2.4469	2.4807
1 0 2	47.48	55.80	56.32	1.8953	1.9134
1 1 0	56.52	66.78	67.27	1.6148	1.6269
1 0 3	62.80	74.54	Not observed	Not observed	Not observed
2 0 0	66.30	78.92	Not observed	Not observed	Not observed
1 1 2	67.88	79.42	Not observed	Not observed	Not observed

[a]NIST SRM 674a certified peak positions for the (1 0 0), (0 0 2), (1 0 1), (1 0 2), (1 1 0), (1 0 3), (2 0 0), and (1 1 2) planes for CuK_α radiation with a wavelength $\lambda = 1.54$ Å.

[b]Certified peak positions, as calculated for CoK_α radiation with a wavelength $\lambda = 1.79$ Å.

[c]Observed NIST SRM 674a peak positions.

[d]Observed NIST SRM 674a *d* spacings.

[e]Corrected NIST SRM 674a *d* spacings (corrected according to the equations in Figure 3B).

and applying the formula

$$G = \frac{m_a}{m_a - m_w} \quad (2)$$

RESULTS AND INTERPRETATIONS

W24N04WA03

Elemental ESEM-EDS analysis of A03 indicates a bulk-rock chemistry consisting largely of Si and Al with lesser K and minor amounts of Ca, Na, Fe, and Ti (Figure 4A). Initially thought to be a pyroxene-plagioclase diabase/gabbro or diorite in hand sample, the presence of measurable potassium revealed through EDS is likely indicative of an intermediate granitoid as opposed to diabase/gabbro/diorite (Nockolds, 1954). Further interpretation of the EDS spectrum indicates that the feldspar component of A03 is a combination of K-feldspar [$KAlSi_3O_8$] and an intermediate plagioclase feldspar (intermediate between the $NaAlSi_3O_8$ [albite] and $CaAl_2Si_2O_8$ [anorthite] end members) and that contributions of calcium and sodium are made from plagioclase and the pyroxene mineral augite [$(Ca,Na)(Mg,Fe,Al)(Si,Al)_2O_6$] or possibly from combinations of plagioclase, pyroxene, and amphibole minerals such as hornblende [$(Ca,Na)_{2-3}(Mg,Fe,Al)_5Si_6(Si,Al)_2O_{22}(OH)_2$]. The presence of Mg-bearing pyroxene and/or amphibole minerals likely accounts for the greenish coloration of the rock observable in hand sample. Accessory minerals consist primarily of minor amounts (less than 3% by volume) of the Fe-Ti oxide mineral ilmenite [$FeTiO_3$] (Figure 5A–C), though the bulk-rock Fe signatures may also be partially derived from amphiboles. Tabular apatite [$Ca_5(PO_4)_3(F,Cl,OH)$] inclusions not visible in hand sample were also detected with EDS in element maps where high concentrations of Ca and P overlap (Figure 5D–F).

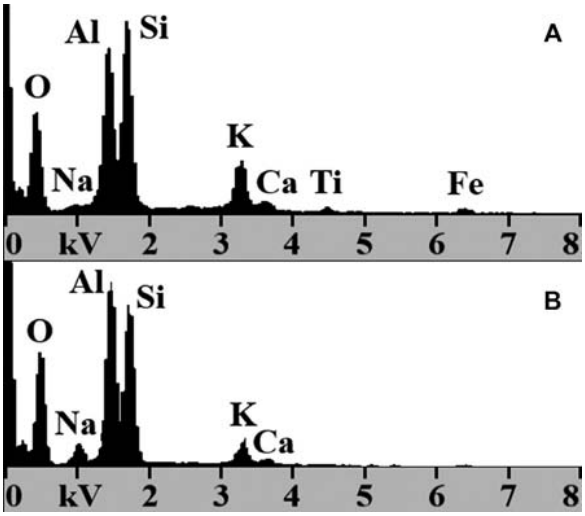

Figure 4 (A) SEM-EDS spectrum of A03, operating with an accelerating voltage of 20.0 kV. The *x*-axis covers the spectrum of energies from 0 to 8 kV, and the *y*-axis is in relative intensity K_α X-rays for O, Na, Al, Si, K, Ca, Ti, and Fe are labeled. (B) SEM-EDS spectrum of A04, operating with an accelerating voltage of 20.0 kV. The *x*-axis covers the spectrum of energies from 0 to 8 kV, and the *y*-axis is in relative intensity K_α X-rays for O, Na, Al, Si, K, and Ca are labeled.

Data obtained from A03 are consistent with a lithologic interpretation of an intermediate, potentially altered, pyroxene- and/or amphibole-bearing granitoid. By definition, "granitoids" are a family of rocks of general granitic composition, which include "true" granites, alkali feldspar granites, granodiorites, and tonalities (Streckeisen, 1973, 1976). Chemically, granitoid rocks display a general trend in which $SiO_2 > Al_2O_3 > K_2O$

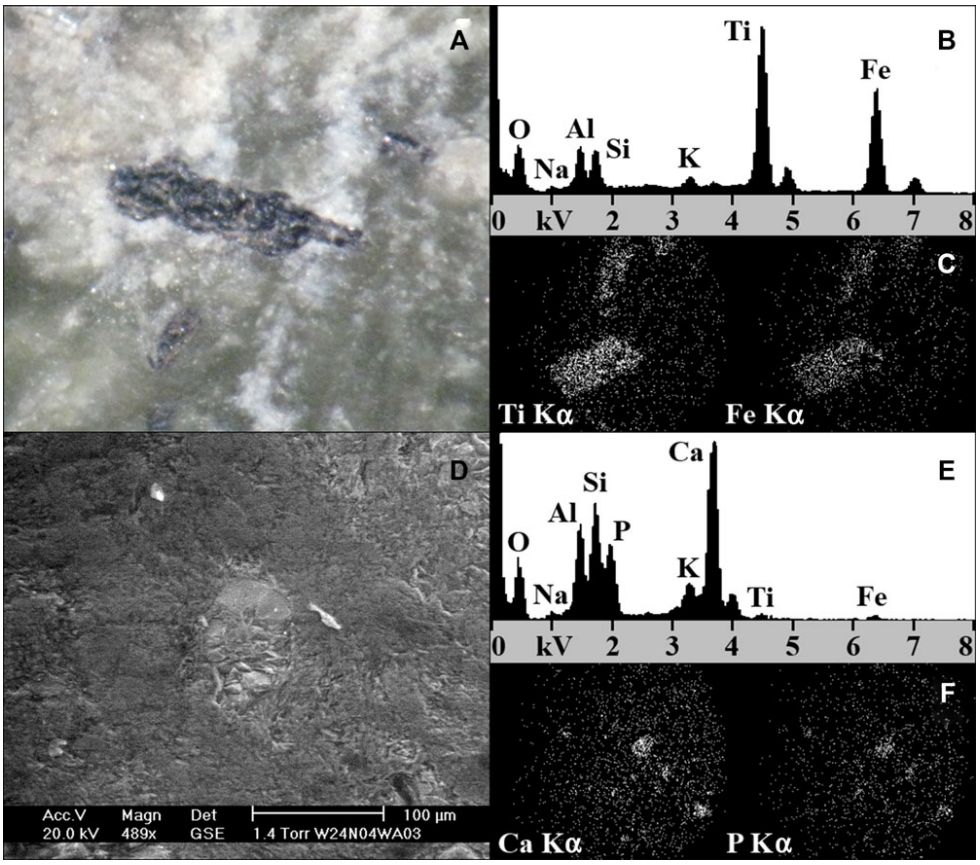

Figure 5 (A) Stereoscopic microscope image of an ilmenite crystal in A03. (B) SEM-EDS spectrum of an ilmenite crystal in A03, operating with an accelerating voltage of 30.0 kV. (C) SEM-EDS element map of an ilmenite crystal in A03, showing K_α X-rays for Ti (left) and Fe (right). (D) Secondary electron image of an apatite crystal in A03. (E) SEM-EDS spectrum of an apatite crystal in A03, operating with an accelerating voltage of 20.0 kV. (F) SEM-EDS element map of an apatite crystal in A03, showing K_α X-rays for Ca (left) and P (right).

$> Na_2O \geq CaO$ (Clarke, 1992). Although not reliably quantifiable in terms of oxide weight percentages, the elemental EDS results from A03 seem to reflect this trend. While classified primarily according to the relative proportions of quartz and feldspars, granitoids, such as those in the southern Appalachian Mountains, also contain minor or accessory amphiboles, pyroxenes, and heavy minerals such as rutile and ilmenite (McSween, Speer, & Fullagar, 1991; Tollo et al., 2004). The lack of observable biotite mica in A03, a common mafic component of granitoid rocks, may be a reflection of (1) relative enrichment of Fe over Mg in the rock (Frost et al., 2001) or (2) the hydrothermal alteration and replacement of biotite with fine-grained chlorite group minerals $[(Mg,Fe)_3(Si,Al)_4O_{10}(OH)_2{\cdot}(Mg,Fe)_3(OH)_6]$ (Fiebig & Hoefs, 2002), the Mg component of which would be undetectable by EDS in a nonvacuum because of the diminished ability of the low-energy Mg X-rays to travel through an atmosphere en route to the detector (Stepon-aitis et al., 2011). The pXRF analysis of A03 measures the concentration of the trace elements Rb, Sr, Y, Zr, and Nb, as well as showing a substantial Fe peak and an appreciable Ti peak (Figure 6A).

Specific gravity measurements of A03 ($G = 2.57$) agree with a granitoid identification. It is important to note, however, that the specific gravity measurement of $G = 2.57$ for A03 represents the most common result obtained over multiple replicate measurements, and that minor variations of 0.1 g in either or both of the mass in air and mass in water resulted in a large range of calculated specific gravities from $G = 2.38$–2.71 (the effect of these minor variations are enhanced by the low mass of A03). Using the specific gravities of quartz ($G = 2.65$), K-feldspars ($G = 2.54$–2.62), plagioclase feldspars ($G = 2.62$–2.76), augite ($G = 3.2$–3.4), hornblende ($G = 3.0$–3.4), apatite ($G = 3.16$–3.22), and ilmenite ($G = 4.7$), and assuming (1) the upper estimate of $G = 2.71$ for A03 and (2) the lower estimates of specific gravity for augite, hornblende, apatite, and the feldspars are applicable, then calculated whole-rock specific gravities of $G = 2.71$ or lower are

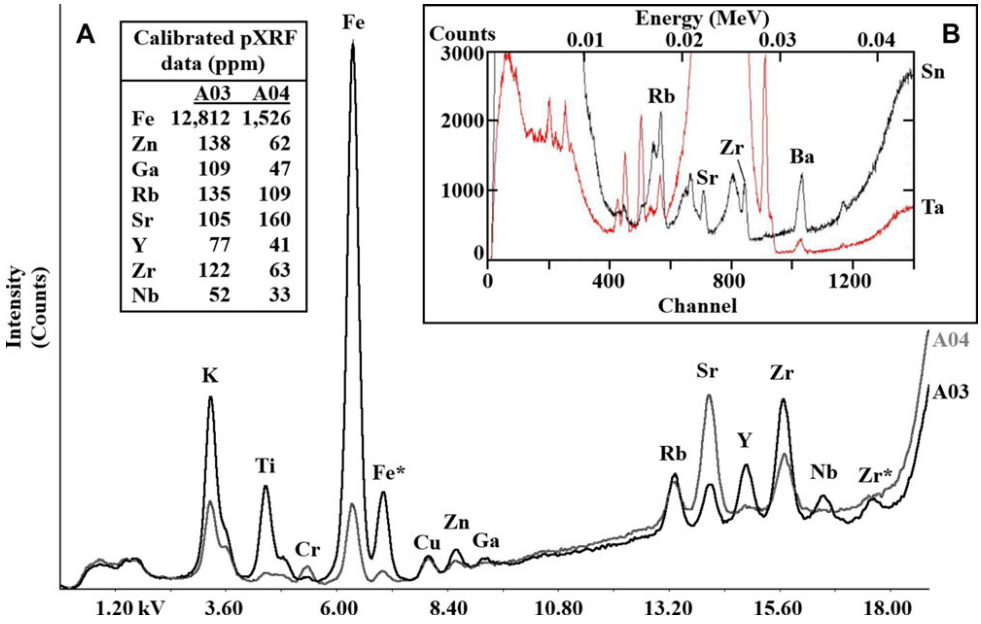

Figure 6 (A) pXRF spectrum of A03 (darker) and A04 (lighter), operating at 40.0 kV and 10.00 μA for 300 seconds. The *x*-axis covers the energy spectrum from 1.20 to 18.00 kV, and the *y*-axis is in relative counts. $K_{\alpha 1}$ spectral lines for K, Ti, Cr, Fe, Cu, Zn, Ga, Rb, Sr, Y, Zr, and Nb are labeled, as well as the $K_{\beta 1}$ spectral lines for Fe and Zr (denoted by an *). The inset at upper left presents the calibrated concentrations (ppm) of selected elements. (B) SUNY—Albany Ion Beam Laboratory XRF spectrum of A04, showing α wave peaks for both the Sn (darker) and Ta (lighter) targets. Peaks corresponding to the α waves of Rb, Sr, Zr, and Ba are labeled.

Table II Calculated whole-rock specific gravities for theoretical granitoids containing the mineral assemblage identified in artifact A03.

Modal composition (%)	Tonalite	Granodiorite	Granite	Pyroxene granite
Quartz	25	30	35	20
Plagioclase	55	35	20	35
K-feldspar	5	25	35	40
Hornblende	10	4	6	1
Augite	3	4	2	2
Ilmenite	1.8	1.8	1.8	1.8
Apatite	0.2	0.2	0.2	0.2
Calc. specific gravity	2.71	2.69	2.68	2.65

Modal mineralogies are roughly based on those presented in Mäkitie et al. (1999), excluding mica phases.

obtainable using modal mineralogies reasonably similar to those presented in Mäkitie et al. (1999) for several possible granitoid compositions (Table II).

W24S04A04

Elemental ESEM-EDS analysis of A04 reveals a bulk-rock chemistry predominantly consisting of Al and Si with lesser amounts of K, Na, and Ca (Figure 4B). Preliminary hand-sample visual examination identified A04 as potentially either a true greenstone or an amphibolite. The minerals typically responsible for imparting the green coloration to greenstones and amphibolites, for example, the chlorite group minerals, serpentine group minerals [$Mg_3Si_2O_5(OH)_4$], or amphibole minerals such as hornblende, actinolite [$Ca_2(Mg,Fe)_5Si_8O_{22}(OH)_2$], or edenite [$NaCa_2Mg_5AlSi_7O_{22}(OH)_2$], are largely magnesian in composition; as previously stated, this is problematic for EDS detection in a nonvacuum. Thus, the requirement to operate the ESEM in an atmosphere did not allow for the detection of Mg, even if it may have been present in the sample. Visual similarities between A04 and a predominantly plagioclase- and edenite-bearing amphibolite/amphibole schist from the Buck Creek mafic/ultramafic complex in the eastern Blue Ridge province of western North Carolina suggests that edenite and plagioclase may constitute the primary mineralogy of A04 (Figure 7). The ESEM-EDS elemental profile may be taken to support this determination. Edenite, unlike other common amphiboles associated with greenstones and amphibolites, lacks stoichiometric Fe. Edenite also contains both stoichiometric Na and Ca, which, unlike Fe, are identifiable in the spectrum. Plagioclase feldspar would also contribute Na and/or Ca to the chemical profile.

This interpretation alone, however, does not account for the high-intensity Al peak and moderate K peak in the spectrum. In addition to the dominant green mineral phase or phases, patches of what appear to be a

Table III Identified peaks in the X-ray diffractogram of A04

$d_{corrected}$	Best Match	Matches within 0.0009 Å
14.2243	chl[a,b]	
9.5888	mica[c]	
9.3097	zeo[b,d]	
5.2903	zeo[b]	
4.9308		
4.7563	pyx[e]	amp[f], chl
4.4018	pyx	mica, KAS[g], chl
4.3559	mica	
4.2440	mica	chl
4.0182	pyx	amp
3.8546		KAS, pl[h], chl, ne[i]
3.7648	clay[j]	mica, zeo, KAS, pl, kfs[k]
3.7105	zeo	
3.6491	pyx	amp
3.4773		zeo, kfs
3.4059	zeo	pl
3.3757	mica	KAS, pl, clay
3.3590	amp	mica, qz[l]
3.3236	zeo	mica, pyx, amp, chl, kfs
3.2605	pl, clay	kfs
3.1991		mica, pyx, pl
3.1539		pyx, KAS, chl, clay
2.9883	pyx, kfs	mica, zeo, chl
2.9196	pyx	mica, pl
2.8638	chl	mica, pyx, pl
2.8203	ZnO[m]	
2.7995	kfs	mica, pyx, zeo, srp[n]
2.6920	KAS	zeo
2.6078	ZnO	
2.5810	mica, kfs	pyx, zeo, KAS, amp, clay, ne
2.5612	amp	mica, pyx, zeo, pl, chl, clay, srp
2.5289	pl	mica, pyx, zeo, amp, chl, clay, kfs, srp
2.4807	ZnO	
2.4661	amp	mica, pyx, zeo, KAS, chl, qz
2.4404		mica, zeo, KAS, pl, amp, chl, ne, srp
2.4293	KAS, pl	mica, pyx, zeo, amp, chl, clay
2.3777	ne	pyx, zeo, KAS, pl, chl, kfs
2.3571	KAS	mica, pyx, zeo, pl, clay
2.3443	ne	mica, pyx, zeo, KAS, amp, clay
2.2499	mica, pyx	zeo, KAS, amp, chl, clay, qz
2.1991	clay	mica, pyx, zeo, KAS, pl, amp, chl, srp
2.1498	srp	mica, pyx, zeo, KAS, amp, clay, ne, srp
2.0025	mica	pyx, KAS, pl, amp, chl, clay, kfs
1.9475	pyx	mica, zeo, KAS, pl, amp, chl, clay, srp
1.9241	mica, pyx	zeo, KAS, pl, amp, kfs, ne, srp
1.9134	ZnO	
1.6817	zeo, KAS, pl, clay	mica, pyx, amp, chl, kfs, srp, qz
1.6269	ZnO	
1.6154	pyx	mica, zeo, KAS, pl, amp, chl, clay, ne
1.6089	mica, pyx	zeo, KAS, pl, amp, clay, ne

[a]chlorite group minerals (chlorite, clinochlore)
[b]best match for a given peak, but not within 0.0009 Å
[c]mica group minerals (muscovite, paragonite, margarite, phengite)
[d]zeolite group minerals (heulandite, stilbite)
[e]pyroxene group minerals (augite, enstatite, diopside, jadeite, omphacite, hypersthene, hedenbergite)
[f]amphibole group minerals (tremolite, actinolite, edenite, anthophyllite)
[g]aluminosilicate group minerals (kyanite, andalusite, sillimanite)
[h]plagioclase group minerals (albite, anorthite)
[i]nepheline
[j]clay group minerals (talc, kaolinite, pyrophyllite)
[k]K-feldspar group minerals (orthoclase, sanidine, microcline)
[l]quartz
[m]NIST SRM 674a
[n]serpentine group minerals (lizardite, antigorite)
Other minerals compared against the data, but not included in Table 2 due to poor matches: calcite, fluorite, corundum, topaz, anatase, rutile, variscite.

Figure 7 Visual comparison of a plagioclase-edenite amphibolite/schist from the Buck Creek mafic/ultramafic complex in Clay County, North Carolina, USA (left) and A04 (right).

white mica phase (e.g., muscovite [$KAl_2(AlSi_3O_{10})(OH)_2$] or margarite [$CaAl_2(Al_2Si_2)_{10}(OH)_2$]) are likely contributing substantial Al and/or K to the elemental profile of A04 (Figure 8C). Additional accessory minerals in A04 include reddish-colored Ti-bearing mineral inclusions interpreted as rutile [TiO_2] on the basis of EDS element maps lacking significant concentrations of Fe in association with the Ti (Figure 8A and B). In some areas, the rutile inclusions grade from a deep red to a reddish-brown and finally to a yellowish-brown phase, possibly indicating differential progression in the stages of alteration or breakdown of the rutile to leucoxene, a common yellow/brown alteration product of Ti-bearing minerals (Allen, 1956; Bailey et al., 1956; Karkhanavala & Momin, 1959; Guilbert & Park, 2007). Also of note are several small embedded monazite [(LREE)PO_4] crystals revealed by EDS to contain significant amounts of the light rare earth elements (LREE) Ce and Nd in association with high concentrations of P and minor amounts of Ca (Figure 8D and E). While monazite often contains minor concentrations of Ca (Flinter, Butler, & Harral, 1963; Zhu & O'Nions, 1999), it is also possible that these crystals are LREE-rich apatites.

The geochemical signature and mineralogical assemblage of A04 is highly suggestive of a lithology similar to the rocks of the Buck Creek complex, in which Berger et al. (2001) identify edenite-margarite schists (hydrothermally altered metatroctolites) with abundant modal plagioclase and strongly elevated LREE signatures. Edenite-bearing assemblages at Buck Creek and other related mafic-ultramafic complexes in western North Carolina (e.g., Tathams Creek and Lake Chatuge) typically contain emerald or grassy-green edenite amphibole (50–70 modal% in combination with magnesiohornblende or pargasite), anorthite (plagioclase, 5–20%), quartz (5–20%) and silvery retrograde margarite, with or without accessory garnet (0–20%), rutile (0–3%), corundum,

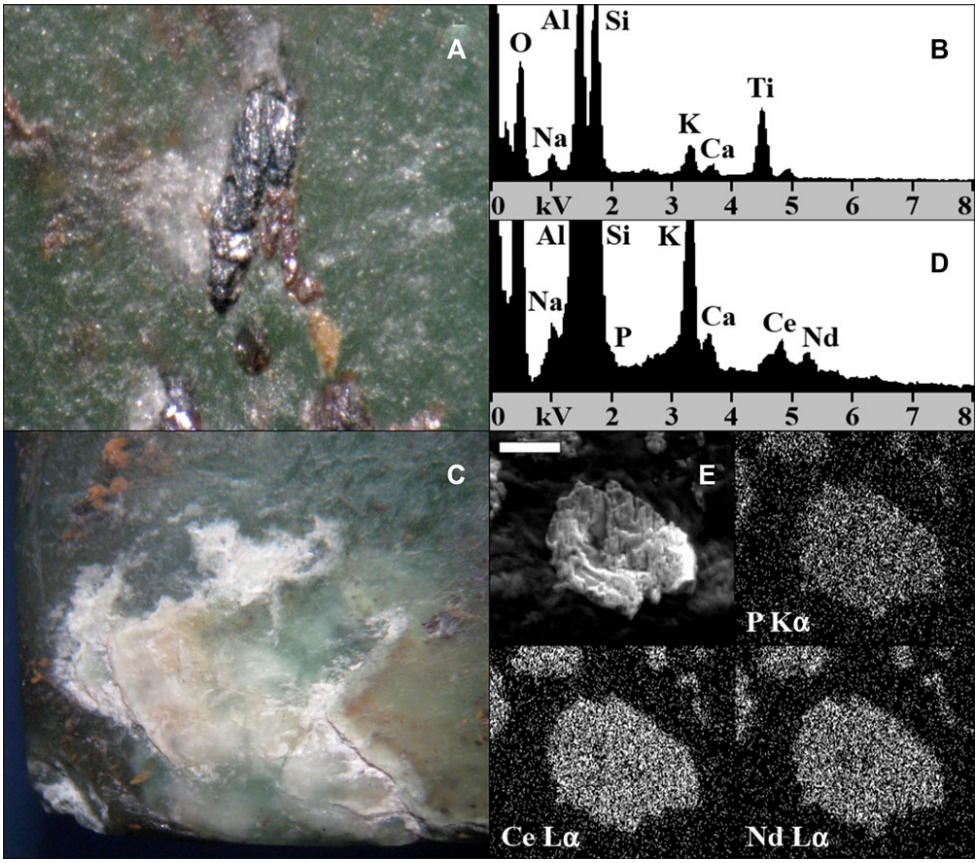

Figure 8 (A) Stereoscopic microscope image of a rutile crystal in A04. (B) SEM-EDS spectrum of a rutile crystal in A04, operating with an accelerating voltage of 20.0 kV. (C) Stereoscopic microscope image of a white mica phase in A04. (D) SEM-EDS spectrum of a monazite crystal in A04, operating with an accelerating voltage of 20.0 kV. (E) Clockwise, from top-left: secondary electron image of a monazite crystal in A03, with 20 μm scale bar in the upper-left; P K_α element distribution map; Nd L_α element distribution map; Ce L_α element distribution map.

augite, spinel, kyanite, zoisite, or chromite (Pratt & Lewis, 1905; Emilio, 1998; Emilio & Ryan, 1998; Peterson & Ryan, 2009; Collins, 2011; Graybeal et al., 2012). Monazite, though not specifically identified in the Buck Creek assemblages, is a common accessory mineral in some hydrothermally altered rocks (Zhu & O'Nions, 1999) and is found in several belts throughout the southeastern Appalachian Piedmont (Mertie, 1979). Despite the potentially varied mineralogy of the amphibolites, Pratt and Lewis (1905) identify assemblages containing only edenite and plagioclase. While A04 lacks any visible foliation suggestive of schist, green aluminous anorthite-bearing edenite amphibolites with accessory chromite, corundum, and spinel were previously identified in the complex by Pratt and Lewis (1905), and Hadley (1949) as alteration products of the troctolite and are equivalent to the edenite-margarite schists of later studies (Peterson & Ryan, 2009); as such, the amphibolite-schist distinction may be of little importance outside of a strictly geological context. While edenite-bearing assemblages are identified in other lithologies throughout the southeastern United States, for example, the Soapstone Ridge metapyroxenite/metaultramafic complex in Georgia (Turner & Swanson, 1998; Chaumba, 2009), the Six Mile thrust sheet, Walhalla nappe, and Chauga belt amphibolites in South Carolina (Prince & Ranson, 2004), granitoids of the Liberty Hill pluton in South Carolina (Speer, 1987), eclogites of the eastern Blue Ridge of North Carolina (Page, Essene, & Mukasa, 2004), and pyroxenites of the Webster-Addie complex in North Carolina (Warner & Swanson, 2010), the edenite is typically subordinate to other amphiboles (actinolite, magnesiohornblende, etc.) or otherwise present only in low modal abundance.

The XRF analysis of A04 conducted at the Ion Beam Laboratory at SUNY—Albany identified trace amounts of Rb, Sr, Zr, and Ba (Figure 6B); pXRF analysis corroborates the concentrations for Rb, Sr, and Zr. Relative to A03, A04 lacks appreciable concentrations of Y and Nb. In addition to these trace elements, the pXRF spectrum also shows lower amounts of Ti and Fe relative to A03

(Figure 6A), which may be significant for sourcing attempts in that Berger et al. (2001) draw chemical distinctions between high-Ti and low-Ti amphibolites in the Buck Creek complex.

The peaks produced from the XRD analysis of A04 (Figure 3A) were corrected and compared against published d spacings for minerals contained within the MSA Crystal Structure Database according to the methods previously outlined. A total of 50 peaks were identified in the diffractogram (Table III). Of the 50 peaks, four are identified as belonging to the ZnO standard. Interpretation of the diffractogram revealed that a combination of the mica, pyroxene, amphibole, and chlorite group minerals, along with plagioclase feldspar, account for 41 of the 46 remaining peaks in the scan. However, four of these five remaining unassigned peaks (at $d = 14.2243$, 9.3097, 5.2903, and 4.9308 Å) are not particularly good matches for any phase and occur at the lower 2θ angles where the least confidence can be placed in the accuracy of the correction. If these peaks are removed from consideration, then a mica-pyroxene-amphibole-chlorite-plagioclase assemblage can explain 40 of 42 assignable peaks in the diffractogram (41 of 43 if the peak at $d = 14.2243$ Å is interpreted as a chlorite peak). With the exception of chlorite, all of these mineral groups have been observed in the edenite-margarite schist/amphibolite of the Buck Creek complex.

In the event that not all of these phases are present in the rock, a simplified white mica-plagioclase-amphibole assemblage (the presumed mineralogy for A04, based on geochemical and petrographic observation) would account for 38 of 42 peaks, while a mica-plagioclase-pyroxene assemblage would account for 39 peaks. The pyroxene group utilized for comparative purposes was an arbitrarily selected subset of seven common, typically green, pyroxene minerals found in the MSA Crystal Structure Database (augite, enstatite, diopside, jadeite, omphacite, hypersthene, hedenbergite); similarly, the four amphibole group minerals selected for comparison (tremolite, actinolite, edenite, anthophyllite) represent only a fraction of the amphibole minerals contained in the MSA database, but are among those associated with green variants. The better fit of the pyroxene-bearing assemblage over the amphibole-bearing assemblage may simply be an effect of more pyroxene data comprising the mineral subsets selected for comparison (seven pyroxenes as opposed to four amphiboles). Thus, preference is given to an amphibole interpretation of the data, as a given amphibole mineral can contribute more, on average, to the explanation of the diffractogram than a given pyroxene. Adding chlorite to the assemblage would explain only one additional peak; in addition to the absence of chlorite in the previously described edenite-bearing rocks, its addition to the assemblage is not necessitated by any significant interpretive improvements. While the zeolite group minerals represent 25 "good" matches (27 if the unassigned peaks at $d = 9.3097$ and 5.2903 Å are attributed to zeolites), their substitution for the micas as the white phase identified in hand sample decreases the overall number of assignable peaks in the simplified plagioclase-amphibole-bearing assemblage from 38 to 37. While the aluminosilicate group minerals have more "good" matches than the amphibole group minerals, and a mica-plagioclase-kyanite assemblage would still explain 38 peaks, this assemblage seems less likely than a mica-plagioclase-amphibole assemblage considering that (1) kyanite is more frequently associated with its blue variant than with its green variant and (2) kyanite is only an accessory phase in the Buck Creek assemblages. Additionally, if the aluminosilicate group is substituted instead for the micas as the white phase seen in hand sample (in this case, sillimanite rather than kyanite), only 36 peaks are assignable. The serpentine group minerals have just nine "good" matches, only one of which is not already afforded by the inclusion of the amphibole group. Neither rutile/leucoxene nor monazite are present in sufficient abundance for XRD detection; Steponaitis et al. (2011) estimate, on the basis of petrographic observation, a detection limit of approximately 10% by volume for any given phase in a non-destructive whole-rock XRD analysis. Quartz, if present (as it is in the rocks of the Buck Creek complex), is either in insufficient quantity to appear in the diffractogram, or the $d = 3.34$ Å reflection is masked by the nearby amphibole reflection at $d = 3.3590$ Å; the absence of the characteristic quartz peak at $d = 3.34$ Å thus precludes a positive identification. While recognizing that there is a fair degree of uncertainty inherent in results stemming from the analysis of a curved sample and that there may be other plausible interpretations of the same diffractogram, a white mica-plagioclase-amphibole assemblage is the simplest assemblage that is well-supported by the XRD data.

Specific gravity determinations may also support the proposed mineral assemblage. The specific gravity measurement of A04 ($G = 2.83$) is an average of eight replicate measurements ranging individually from $G = 2.73$–2.93; six replicate specific gravity measurements of the Buck Creek plagioclase-edenite sample utilized for visual comparison ranged from $G = 2.75$–2.93, also averaging $G = 2.83$. A general Buck Creek assemblage of 60% edenite ($G = 3.0$), 20% anorthite ($G = 2.76$), 10% white mica ($G = 2.8$), 8% quartz ($G = 2.65$), and 2% rutile ($G = 4.2$) yields a calculated specific gravity of $G = 2.93$. Excluding quartz, a specific gravity of $G = 2.93$ or less is easily obtainable with assemblages reasonably similar to those of the Buck Creek complex (e.g., 53% edenite, 25%

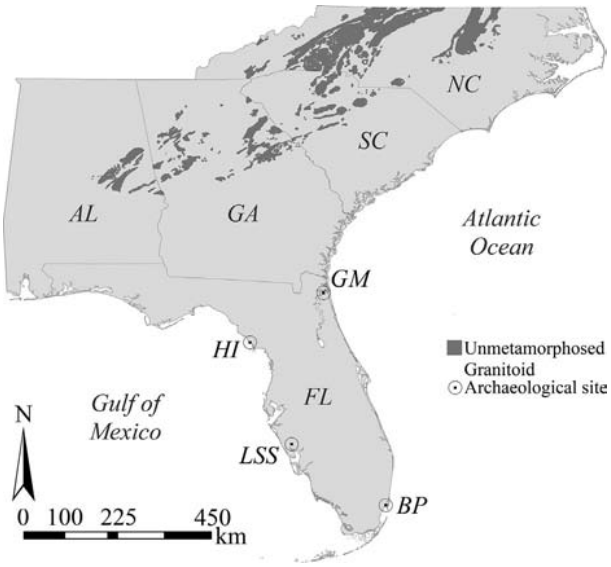

Figure 9 Potential unmetamorphosed granitoid sources for A03. *LSS* = Little Salt Spring (8SO18); *BP* = Brickell Point (8DA12); *HI* = Hog Island/Grave Yard Island (8CI220); *GM* = Goodman Mound.

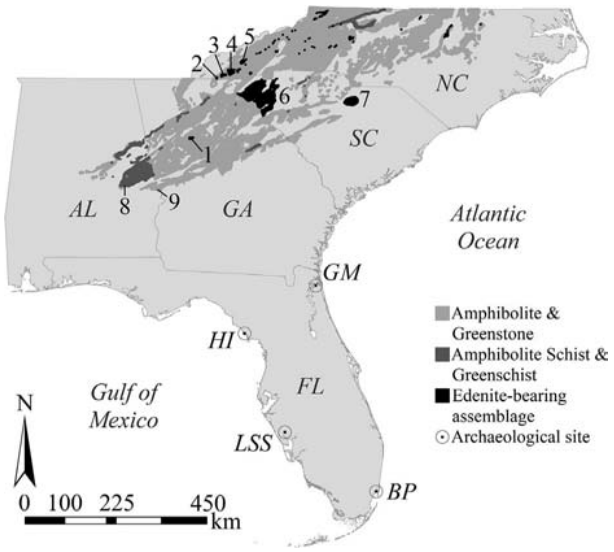

Figure 10 Potential amphibolite, greenstone, amphibole-bearing schist, and edenite-bearing sources for A04, with sources mentioned in text (approximate distance for select sources from Little Salt Spring provided in parentheses): 1 = Soapstone Ridge complex (755 km); 2 = Lake Chatuge complex; 3 = Buck Creek complex (895 km); 4 = Carroll Knob complex; 5 = Webster-Addie complex; 6 = Six Mile thrust sheet, Walhalla nappe, Chauga belt; 7 = Liberty Hill pluton; 8 = Dadeville complex (695–740 km); 9 = Uchee complex (660 km). *LSS* = Little Salt Spring (8SO18); *BP* = Brickell Point (8DA12); *HI* = Hog Island/Grave Yard Island (8CI220); *GM* = Goodman Mound.

anorthite, 20% white mica, 2% rutile yields $G = 2.92$). Pyroxenes, in general, have higher specific gravities than amphiboles ($G = 3.2$ would be a relatively low estimate with respect to many common pyroxenes), making it more difficult to justify the replacement of amphiboles with pyroxenes in the proposed assemblage.

CONCLUSIONS

Exotic ceremonial stone pendants recovered from the Archaic-period Little Salt Spring site in Florida were identified as a potentially altered, coarse-grained intermediate pyroxene- and/or amphibole-bearing granitoid, and an altered edenite amphibolite or amphibole schist through a combination of non-destructive hand-sample petrography, ESEM-EDS, whole-rock XRD, and specific gravity determinations. Geologic units matching these general lithologies were identified through an exhaustive search of all lithologic units entered for the southeastern states of North Carolina, South Carolina, Georgia, Alabama, and Florida in the United States Geological Survey's (USGS) National Geologic Map Database lithologic search tool GEOLEX (http://ngmdb.usgs.gov/Geolex/; USGS, 2012a) and Mineral Resources On-Line Spatial Data GIS database of geologic units (http://mrdata.usgs.gov/geology/state/; USGS, 2012b). These units, representing the most likely potential sources for the Little Salt Spring artifacts, are displayed in Figure 9 (for all unmetamorphosed granitoid lithologies in Alabama, Georgia, South Carolina, and North Carolina) and Figure 10. In Figure 10, units are mapped according to the relative levels of confidence placed on each as a potential source for artifact A04. The most likely units (mapped in the darkest shade) are those in which edenite has been explicitly identified as an amphibole phase in the geological literature (e.g., Buck Creek and Soapstone Ridge). Moderate likelihoods are placed on units with the same general lithologic associations as the Buck Creek complex and other edenite-bearing units, that is, amphibolites occurring in association with amphibole-bearing schists, amphibole-bearing schists, schists with mineral assemblages indicative of greenschist facies metamorphism (e.g., actinolite, chlorite, talc, etc.), or ultramafic complexes; these units are displayed in an intermediate shade in Figure 10. Lastly, generic amphibolite units (i.e., not in direct association with amphibole-bearing schists) are considered less-probable, though possible, sources and are displayed in the lightest shade.

The simplest hypothesis on the provenance of the stones from which pendants A03 and A04 had been fashioned would source the material to the closest available source or sources to where they were recovered at Little Salt Spring, as per Earle and Ericson's (1977: 6–7) assertion that in cases involving raw materials with either few or closely clustered sources, it is "sufficient to

assume that material . . . came from the nearest source." The Florida Peninsula, however, is notoriously devoid of any appreciable amount of "hard" (i.e., noncarbonate) rock; there are no known outcrops of granitoids, amphibolites, amphibole-schists, or ultramafic rocks within the state of Florida. While large-scale Middle Archaic chert quarries and tool workshops associated with major outcrops such as the Senator Edwards and Johnson Lake sites in Marion County are known in Florida, there is not much else in terms of workable stone (Milanich & Fairbanks, 1980: 58; Milanich, 1998: 22). For this reason, the presence of exotic stone artifacts in Florida has generally been attributed to exchange or trade with regions to the north (Dixon et al., 2000). The closest granitoid outcrops to the north of Little Salt Spring that represent potential source rocks for A03 are found in the Georgia and Alabama Piedmont at a minimum distance of 650–660 km from the site (Figure 9). With respect to A04, the closest edenite-bearing assemblages to Little Salt Spring are the mafic/ultramafic rocks of the Soapstone Ridge complex in the Georgia Piedmont (755 km distant; "1" in Figure 10), while the Buck Creek complex ("3") is approximately 895 km from Little Salt Spring. The closest lithologic associations resembling those of the Buck Creek complex are in the Dadeville complex of the Alabama Piedmont between 695 and 740 km from Little Salt Spring ("8"). General amphibolite units, the most geographically widespread units under consideration as potential source rocks for A04, occur at a minimum distance of 650 km from Little Salt Spring in the Georgia Piedmont. While there is no evidence to suggest any close temporal or geographic relation between the two pendants, the closest localities in which potential sources exist for both A03 and A04 within the same unit occur in the Uchee complex of the Alabama Piedmont, approximately 660 km from Little Salt Spring ("9").

South of the Florida Peninsula, ultramafic complexes, jadeitite deposits, serpentinite bodies, and amphibolites notably outcrop along Cuba's and Hispaniola's northern coasts (Iturralde-Vinent, 1994; García-Casco et al., 2009) and within Guatemala's Motagua fault zone (Harlow, Sorenson, & Sisson, 2007). The occurrence of the proposed mica-plagioclase-edenite assemblage for artifact A04 in particular is common in central and eastern Cuba's amphibolite complexes (e.g., the Mabujina and Güira de Juaco complexes), as is the occurrence of amphibole-bearing granitoids (with respect to A03) in central Cuba's Santa Clara—Camaguey regions (Garcia-Casco, personal communication, 2013). While Cuba's northernmost ultramafic deposits occur at a distance of less than 500 km from Little Salt Spring—at least 150 km nearer than comparable lithologies in the Appalachian Piedmont—and while lithic sourcing has provided evidence for pre-Columbian long-distance trans-Caribbean maritime exchange networks—jadeitite artifacts from Guatemala are proposed to have traveled over 2700 km to the islands of the Lesser Antilles (Harlow et al., 2006; Garcia-Casco et al., 2013)—there is, to date, no conclusive archaeological evidence that prehistoric Florida was engaged in maritime-based exchange with either the Caribbean or Mesoamerica (Dixon et al., 2000). Though the earliest estimate of the settlement of the Caribbean islands (Cuba by 6000 B.P.; Fitzpatrick & Keegan, 2007) is contemporaneous with the Archaic occupations at Little Salt Spring, it is highly unlikely that any maritime exchange networks linking Florida and Cuba would have been established this early in the settlement history of the Caribbean. Polished stone artifacts do not appear in Cuba's Archaic assemblages (Garcia-Casco, personal communication, 2013) at all, and only at other sites in the Greater Antilles several millennia later.

More precise determinations of provenance beyond the general potential source regions presented here may not be possible for either artifact given the qualitative nature of the data and the lack of comparable geological reference samples. Given the scope of the present research, undertaken largely as an exploratory analysis, it was not possible to extensively collect and analyze reference samples from these identified potential sources. Regardless of whether a single "best" source can be identified among these geographically widespread potential sources, it makes little difference with respect to the broader archaeological interpretation. In the case of the Little Salt Spring greenstone pendants, even the "best" source among those identified must occur at a minimum distance of 650 km to the north of the site in the southern Appalachian Piedmont. Given these distances, a direct access model of acquisition is unlikely. According to Milanich and Fairbanks (1980: 19), Florida's Archaic peoples were becoming "increasingly sedentary collectors and gatherers," occupying a single campsite for an appreciable portion of the year. The Early Archaic peoples were "viewed as a population changing from the nomadic Paleoindian subsistence pattern to the more settled coastal- and riverine-associated regimes of the Middle Archaic Period" (Milanich, 1994: 63–64). While Middle Archaic peoples were thought to travel out from large villages or camp sites on hunting trips and to collect resources (Milanich, 1998: 21), ethnographic studies by Kelly (1983) place an upper limit to the annual linear distance covered by modern hunter-gatherer groups at 800 km, with a majority of those groups traveling no more than 200–300 km per year. A direct-access model of acquisition would require a minimum roundtrip distance of 1300 km from Little Salt Spring to the nearest available source. A more plausible interpretation is that a

long-distance exchange/distribution network for critical resources was in place during the Archaic and resulted in the importation, albeit on a limited basis, of exotic stone resources from the southern Appalachian Piedmont deep into central and southern Florida. The scarcity of these exotic lithic materials at Little Salt Spring argue against such a network having a particularly large scale or sustained nature, following Daniel's (2001) conclusion that Archaic band societies in the southeastern United States were most likely incapable of supplying stone resources *in bulk* to other groups. This, however, would not preclude an alternative model of a system of down-the-line exchange of *small volumes* of high-status objects fabricated from rare (with respect to the geology of Florida) lithic raw materials of presumed prestige value.

Such long-distance terrestrial exchange networks are identifiable in later archaeological contexts across the state of Florida. For example, Dixon et al. (2000) sourced Late Woodland/Mississippian period (A.D. 500–1685) basaltic groundstone celts from the Brickell Point archaeological site in Miami to the basaltic dikes near Atlanta and Macon in the Georgia Piedmont (over 850 km distant from Brickell Point). Black (1971), though making no provenance determination, identified a Late Woodland period greenstone celt from a site just north of Cedar Key (the Hog Island/Grave Yard Island site, approximately 250 km northwest of Little Salt Spring) as an indisputable trade item; the nearest potential sources for this artifact would occur at least 400 km to the north in the Georgia Piedmont. Recourt (1975) similarly concluded that a greenstone celt excavated at the Goodman mound site in northern Florida (dating from the St. Johns I culture, following the Late Archaic) represents a trade item originating in northern Georgia. The preliminary provenance determination of the Archaic period Little Salt Spring greenstones, as presented here, would definitively place the origins of the south and central Florida—Appalachian Piedmont lithic exchange network at least as far back as the Middle Archaic. While the ability to interpret the given data is largely a function of the peculiar geological nature of the Florida Peninsula, the preceding study nevertheless illustrates (1) the potential utility of non-destructive ESEM- and XRD-based methodologies for deriving meaningful archaeological conclusions from analyses conducted under traditionally nonideal analytical conditions and (2) the greater interpretive power afforded by the synthesis of basic geochemical, petrographic, and lithologic data in provenance investigations.

The authors wish to thank all those involved in supporting this study, particularly Terri Hood and Husain Al Sayegh for their assistance in collecting and interpreting the ESEM-EDS data, and the number of editors and reviewers, both named (Gary Huckleberry, Jamie Woodward, Sam Swanson) and anonymous, whose comments, suggestions, and insights significantly improved the quality of the manuscript. Antonio Garcia-Casco, Jacqueline Dixon, Patricia Blackwelder, Steven Koski, Paul Schroeder, Stephen Kowalewski, Michael Roden, William Lanford, Arthur Haberl, Doug Dvoracek, Manuel Iturralde-Vinent, Albert Hine, Sara Elliott, Gail Tarver, and Nicole Lipson are also deserving of individual recognition for providing additional insight and references and for their contributions and assistance in analysis, interpretation, and proofreading.

REFERENCES

Allen, V.T. (1956). Is leucoxene always finely crystalline rutile? Economic Geology, 51, 830–833.

Artioli, G., & Angelini, I. (2011). Mineralogy and archaeometry: Fatal attraction. European Journal of Mineralogy, 23, 849–855.

Bailey, S.W., Cameron, E.N., Spedden, H.R., & Weege, R.J. (1956). The alteration of ilmenite in beach sands. Economic Geology, 51, 263–279.

Berger, S., Cochrane, D., Simons, K., Savov, I., Ryan, J.G., & Peterson, V.L. (2001). Insights from rare earth elements into the genesis of the Buck Creek complex, Clay County, NC. Southeastern Geology, 40(3), 201–212.

Bertin, E.P. (1970). Principles and practice of X-ray spectrometric analysis. New York: Plenum Press.

Black, D.A. (1971). An extremely long celt. Florida Anthropologist, 24, 44.

Burke, A. (2006). Paleoindian ranges in northeastern North America based on lithic raw materials sourcing. In C. Bressy, A. Burke, P. Chalard, & H. Martin (Eds.), Notions de Territoire et de Mobilité: Exemples de l'Europe et des Premières Nations en Amérique du Nord Avant le Contact Européen. Actes de Sessions Présentée sau Xe Congrès Annual de l'Association Européen ne des Archéologues (Lyon, 8–11 Septembre 2004). Etudes et Recherches Archéologiques de l'Université de Liège (ERAUL), Vol. 116 (pp. 1–14). Liège, Belgium: Université de Liège.

Chaumba, J.B. (2009). The Soapstone Ridge Complex, Southern Appalachians; a petrographical, mineral compositional, and oxygen isotope investigation. Geological Society of America Abstracts with Programs, 41, 662.

Clarke, D.B. (1992). Granitoid rocks. New York: Chapman & Hall.

Clausen, C.J., Cohen, A.D., Emiliani, C., Holman, J.A., & Stipp, J.J. (1979). Little Salt Spring, Florida: A unique underwater site. Science, 203, 609–614.

Collins, N. (2011). Geochemical systematics among amphibolitic rocks in the Central Blue Ridge Province of southwestern North Carolina. Unpublished master's thesis, University of South Florida, Tampa.

Daniel, I.R., Jr. (2001). Stone raw material availability and early Archaic settlement in the southeastern United States. American Antiquity, 66, 237–265.

Danilatos, G.D. (1991). Review and outline of environmental SEM at present. Journal of Microscopy, 162, 391–402.
Dixon, J.E., Simons, K., Leist, L., Eck, C., Ricisak, J., Gifford, J.A., & Ryan, J. (2000). Provenance of stone celts from the Miami Circle Archaeological Site, Miami, Florida. Florida Anthropologist, 53, 328–341.
Downs, R.T., & Hall-Wallace, M. (2003). The American mineralogist crystal structure database. American Mineralogist, 88, 247–250.
Earle, T.K., & Ericson, J.E. (1977). Exchange systems in archaeological perspective. In T.K. Earle & J.E. Ericson (Eds.), Exchange systems in prehistory (pp. 3–12). New York: Academic Press.
Emilio, M.C. (1998). Metamorphic evolution of the Buck Creek mafic-ulltramafic complex, Clay County, North Carolina, USA. Unpublished master's thesis, University of South Florida, Tampa.
Emilio, M., & Ryan, J. (1998). P-T history and structural controls on the Buck Creek mafic-ultramafic complex, eastern Blue Ridge, North Carolina. Geological Society of America Abstracts with Programs, 30, 380.
Fiebig, J., & Hoefs, J. (2002). Hydrothermal alteration of biotite and plagioclase as inferred from intragranular oxygen isotope- and cation-distribution patterns. European Journal of Mineralogy, 14, 49–60.
Fitzpatrick, S.M., & Keegan, W.F. (2007). Human impacts and adaptations in the Caribbean Islands: An historical ecology approach. Earth and Environmental Science Transactions of the Royal Society of Edinburgh, 98, 29–45.
Flinter, B.H., Butler, J.R., & Harral, G.M. (1963). A study of alluvial monazite from Malaya. American Mineralogist, 48, 1210–1226.
Freestone, I.C., & Middleton, A.P. (1987). Mineralogical applications of the analytical SEM in archaeology. Mineralogical Magazine, 51, 21–31.
Frost, B.R., Barnes, C.G., Collins, W.J., Arculus, R.J., Ellis, D.J., & Frost, C.D. (2001). A geochemical classification for granitic rocks. Journal of Petrology, 42, 2033–2048.
Garcia-Casco, A., Knippenberg, S., Rodríguez Ramos, R., Harlow, G.E., Hofman, C., Carlos Pomo, J., & Blanco-Quintero, I.F. (2013). Pre-Columbian jadeitite artifacts from Elliot's, Antigua: Implications for potential source regions and long-distance exchange networks in the Greater Caribbean. Journal of Archaeological Science, 40, 3153–3169.
García-Casco, A., Vega, A.R., Párraga, J.C., Iturralde-Vinent, M.A., Lázaro, C., Quintero, I.B., Agramonte, Y.R., Kröner, A., Cambra, K.N., Millán, G., Torres-Roldán, R.L., & Carrasquilla, S. (2009). A new jadeitite jade locality (Sierra del Convento, Cuba): First report and some petrological and archeological implications. Contributions to Mineralogy and Petrology, 158, 1–16.
Gifford, J.A. (1993). Videography and geographical information systems for recording the excavation of a prehistoric underwater site. International Journal of Nautical Archaeology, 22, 167–172.
Graybeal, D.B., Kiel, N.J., Dyer, E.K., Kling, C.L., Perez, A.E., Sellers, R.C., Foster, N.A., Fleisher, C.J., & Swanson, S.E. (2012). Mineralogy of the oxide minerals in the Buck Creek mafic-ultramafic complex, North Carolina. Geological Society of America Abstracts with Programs, 44, 244.
Guilbert, J.M., & Park, C.F., Jr. (2007). The geology of ore deposits. Long Grove, IL: Waveland Press, Inc.
Hadley, J.B. (1949). Preliminary report on corundum deposits in the Buck Creek peridotite, Clay County, N. C. Bulletin 948-E. Washington, DC: United States Department of the Interior.
Harlow, G.E., Murphy, A.R., Hozjan, D.J., de Mille, C.N., & Levinson, A.A. (2006). Pre-Columbian jadeite axes from Antigua, West Indies: Description and possible sources. Canadian Mineralogist, 44, 305–321.
Harlow, G.E., Sorensen, S.S., & Sisson, V.B. (2007). Jade. In L.A. Groat (Ed.), Geology of gem deposits: Short course series Vol. 37 (pp. 207–253). Yellowknife: Mineralogical Association of Canada.
Hermes, O.D., & Ritchie, D. (1997). Nondestructive trace element analysis of archaeological felsite by energy-dispersive X-ray fluorescence spectroscopy. Geoarchaeology, 12, 31–40.
Hurst, V.J., Schroeder, P.A., & Styron, R.W. (1997). Accurate quantification of quartz and other phases by powder X-ray diffractometry. Analytica Chimica Acta, 337, 233–252.
Iturralde-Vinent, M.A. (1994). Cuban geology: A new plate-tectonic synthesis. Journal of Petroleum Geology, 17, 39–70.
Janssens, K., Vittiglio, G., Deraedt, I., Aerts, A., Vekemans, B., Vincze, L., Wei, F., Deryck, I., Schalm, O., Adams, F., Rindby, A., Knöchel, A., Simionovici, A., & Snigirev, A. (2000). Use of microscopic XRF for non-destructive analysis in art and archaeometry. X-Ray Spectrometry, 29, 73–91.
Karkhanavala, M.D., & Momin, A.C. (1959). The alteration of ilmenite. Economic Geology, 54, 1095–1102.
Kelly, R.L. (1983). Hunter-gatherer mobility strategies. Journal of Anthropological Research, 39, 277–306.
Klein, C. (2002). Manual of mineral science, 22nd ed. United States: John Wiley & Sons, Inc.
Kuhn, R.D., & Lanford, W.A. (1987). Sourcing Hudson Valley cherts from trace element analysis. Man in the Northeast, 34, 57–69.
Lundblad, S.P., Mills, P.R., & Hon, K. (2008). Analysing archaeological basalt using non-destructive energy-dispersive X-ray fluorescence (EDXRF): Effects of post-depositional chemical weathering and sample size on analytical precision. Archaeometry, 50, 1–11.
Mäkitie, H., Kärkkäinen, N., Lahti, S.I., & Lehtonen, M.I. (1999). Chemical and modal composition of granitoids in three different geological units, South-Pohjanmaa, western

Finland. Special Paper 27. Espoo: Geological Survey of Finland.
Mantler, M., & Schreiner, M. (2000). X-ray fluorescence spectrometry in art and archaeology. X-Ray Spectrometry, 29, 3–17.
McSween, H.Y., Jr., Speer, J.A., & Fullagar, P.D. (1991). Plutonic rocks. In J.W. Horton, Jr. & V.A. Zullo (Eds.), The geology of the Carolinas (pp. 109–126). Knoxville: University of Tennessee Press.
Mertie, J.B., Jr. (1979). Monazite in the granitic rocks of the southeastern Atlantic states—An example of the use of heavy minerals in geologic exploration. Professional Paper 1094. Washington, DC: United States Geological Survey.
Michelaki, K., Hancock, R.G.V., & Braun, G.V. (2012). Using provenance data to assess archaeological landscapes: An example from Calabria, Italy. Journal of Archaeological Science, 39, 234–246.
Milanich, J.T. (1994). Archaeology of Precolumbian Florida. Gainesville: University Press of Florida.
Milanich, J.T. (1998). Florida's Indians from ancient times to the present. Gainesville: University Press of Florida.
Milanich, J.T., & Fairbanks, C.H. (1980). Florida archaeology. New York: Academic Press.
Mineralogical Society of America (2013). The American Mineralogist Crystal Structure Database. <www.minsocam.org/msa/crystal_database.html>.
Moore, D.M., & Reynolds, R.C., Jr. (1997). X-ray diffraction and the identification and analysis of clay minerals. New York: Oxford University Press.
Nazaroff, A.J., Baysal, A., & Çiftçi, Y. (2013). The importance of chert in Central Anatolia: Lessons from the Neolithic assemblage at Çatalhöyük, Turkey. Geoarchaeology, 28, 340–362.
Neff, H. (2012). Comment: Chemical and mineralogical approaches to ceramic provenance determination. Archaeometry, 54, 244–249.
Nevin, A., Spoto, G., & Anglos, D. (2012). Laser spectroscopies for elemental and molecular analysis in art and archaeology. Applied Physics A, 106, 339–361.
Nockolds, S.R. (1954). Average chemical compositions of some igneous rocks. Bulletin of the Geological Society of America, 65, 1007–1032.
Page, F.Z., Essene, E.J., & Mukasa, S.B. (2004). Quartz exsolution in clinopyroxene is not proof of ultra-high pressures: Evidence from phase equilibria and eclogite from the eastern Blue Ridge, southern Appalachians, USA. Geological Society of America Abstracts with Programs, 36, 453.
Parish, R.M., Swihart, G.H., & Li, Y.S. (2013). Evaluating Fourier transform infrared spectroscopy as a non-destructive chert sourcing technique. Geoarchaeology, 28, 289–307.
Peterson, V., & Ryan, J.G. (2009). Petrogenesis and structure of the Buck Creek mafic-ultramafic suite, southern Appalachians: Constraints on ophiolite evolution and emplacement in collisional orogens. Geological Society of America Bulletin, 121, 615–629.
Potts, P.J. (1987). A handbook of silicate rock analysis. New York: Chapman & Hall.
Potts, P.J. (2008). Introduction, analytical instrumentation and application overview. In P.J. Potts & M. West (Eds.), Portable X-ray fluorescence spectrometry: Capabilities for in situ analysis (pp. 1–12). Cambridge: The Royal Society of Chemistry.
Potts, P.J., & West, M. (2008). Portable X-ray fluorescence spectrometry: Capabilities for in situ analysis. Cambridge: The Royal Society of Chemistry.
Pratt, J.H., & Lewis, J.V. (1905). Corundum and the peridotites of western North Carolina. Raleigh: North Carolina Geological Survey.
Prince, P.S., & Ranson, W.A. (2004). Geochemistry, petrography, and mineral chemistry of amphibolites from the Inner Piedmont of northwestern South Carolina. Geological Society of America Abstracts with Programs, 36, 103.
Rapp, G. (2009). Archaeomineralogy, 2nd ed. Berlin: Springer.
Recourt, P. (1975). Final notes on the Goodman mound. Florida Anthropologist, 28, 85–95.
Šegvić, B., Šešelj, L., Slovenec, D., Lugović, B., & Mählmann, R.F. (2012). Composition, technology of manufacture, and circulation of hellenistic pottery from the Eastern Adriatic: A case study of three archaeological sites along the Dalmatian Coast, Croatia. Geoarchaeology, 27, 63–87.
Shotton, F.W., & Hendry, G.L. (1979). The developing field of petrology in archaeology. Journal of Archaeological Science, 6, 75–84.
Shugar, A.N., & Mass, J.L. (2012). Studies in archaeological sciences: Handheld XRF for art and archaeology. Leuven: Leuven University Press.
Speer, J.A. (1987). Evolution of magmatic AFM mineral assemblages in granitoid rocks: The hornblende + melt = biotite reaction in the Liberty Hill pluton, South Carolina. American Mineralogist, 72, 863–878.
Środoń, J, Drits, V.A., McCarty, D.K., Hsieh, J.C.C., & Eberl, D.D. (2001). Quantitative X-ray diffraction analysis of clay-bearing rocks from random preparations. Clays and Clay Minerals, 49, 514–528.
Steponaitis, V.P., Swanson, S.E., Wheeler, G., & Drooker, P.B. (2011). The provenance and use of Etowah palettes. American Antiquity, 76, 81–106.
Stevenson, C.M., Klimkiewicz, M., & Scheetz, B.E. (1990). X-ray fluorescence analysis of jaspers from the Woodward Site (36CH374), the Kasowski Site (36CH161), and selected eastern United States jasper quarries. Journal of Middle Atlantic Archaeology, 6, 43–54.
Stoltman, J.B., Marcus, J., Flannery, K.V., Burton, J.H., & Moyle, R.G. (2005). Petrographic evidence shows that

pottery exchange between the Olmec and their neighbors was two-way. Proceedings of the National Academy of Sciences of the United States of America, 102, 11213–11218.

Streckeisen, A.L. (1973). Plutonic rocks, classification and nomenclature recommended by the IUGS subcommission on the systematics of igneous rocks. Geotimes, 18, 26–30.

Streckeisen, A.L. (1976). To each plutonic rock its proper name. Earth-Science Reviews, 12, 1–33.

Tollo, R.P., Aleinikoff, J.N., Bartholomew, M.J., & Rankin, D.W. (2004). Neoproterozoic A-type granitoids of the central and southern Appalachians: Intraplate magmatism associated with episodic rifting of the Rodinian supercontinent. Precambrian Research, 128, 3–38.

Turner, A.V., & Swanson, S. (1998). A mineralogical and geochemical comparison of two Native American soapstone quarries. Geological Society of America Abstracts with Programs, 30, 17.

United States Geological Survey (2012a). National Geologic Map Database: Geologic Names Lexicon, "GEOLEX." <ngmdb.usgs.gov/Geolex/>.

United States Geological Survey (2012b). Mineral Resources On-Line Spatial Data: Geologic maps of US states. <mrdata.usgs.gov/geology/state>.

Vicens, E., Arribas, M.A., Clop, X., Estrada, M.R., Maestro, E., Oms, O., Serrat, D., & Molist, M. (2010). Characterization and provenance of the slabs of the Puigseslloses Megalith, Barcelona, Spain. Geoarchaeology, 25, 195–219.

Warner, R.D., & Swanson, S.E. (2010). Metamorphism of cpx-rich rocks from Webster-Addie ultramafic complex. Southeastern Geology, 47, 123–145.

Wentz, R.K., & Gifford, J.A. (2007). Florida's deep past: The bioarchaeology of Little Salt Spring (8SO18) and its place among mortuary ponds of the Archaic. Southeastern Archaeology, 26, 330–337.

Williams-Thorpe, O., Potts, P.J., & Webb, P.C. (1999). Field-portable non-destructive analysis of lithic archaeological samples by X-ray fluorescence instrumentation using a mercury iodide detector: Comparison with wavelength-dispersive XRF and a case study in British stone axe provenancing. Journal of Archaeological Science, 26, 215–237.

Zhigachev, A.O. (2013). The effect of specimen surface curvature on X-ray diffraction peak profiles. Review of Scientific Instruments, 84, 095105, 1–8.

Zhu, X.K., & O'Nions, R.K. (1999). Monazite chemical composition: Some implications for monazite geochronology. Contributions to Mineralogy and Petrology, 137, 351–363.

